



## Effective Deep Learning Network Model for Multi-Class Skin Cancer Classification

Vankayalapati Radhika<sup>1</sup>      B. Sai Chandana<sup>1\*</sup>

<sup>1</sup>*School of Computer Science and Engineering, VIT-AP University, Amaravati, Andhra Pradesh, 522237, India*

\* Corresponding author's Email: saichandanas869@gmail.com

---

**Abstract:** Skin cancer is a prevalent condition that may affect anybody, regardless of age. To lower the fatality rate by catching diseases in their earliest stages, automated skin cancer detection is required. In recent years, skin cancer screening and detection have become more popular due to the imaging-based computer-aided diagnosis (CAD) approach. To identify and classify skin lesions, this research developed an automated integrative deep-learning network model. The hair is removed using a dull razor approach, and the noise is removed using an average median filter during image pre-processing. The afflicted lesion regions are found in the dermoscopic images using the Otsu thresholding approach and mathematical morphology. From the segmented lesions, the significant features are extracted using improved capsule network (Improved CapsNet). Finally, the enhanced optimized probabilistic neural network (EOPNN) is used for skin lesion classification. The improved artificial jelly optimization (IAJO) algorithm enhances the EOPNN classifier. A benchmark ISIC dataset is used to validate the proposed EOPNN-IAJO approach. The proposed structure has achieved encouraging results for several metrics with 99.23% specificity, 99.02% sensitivity, and 99.53% accuracy.

**Keywords:** Skin cancer, Dull razor approach, Median filter, Otsu thresholding, Improved CapsNet, Improved artificial jelly optimization.

---

### 1. Introduction

The most fatal kind of cancer in the world is skin cancer [1]. Intraepithelial carcinoma, squamous cell carcinoma, basal cell carcinoma, melanoma, and other types of skin cancer exist worldwide [2]. The epidermis, dermis, and hypodermis are the three tissue layers that make up human skin [3]. Melanocytes found in the epidermal layer may occasionally produce excessive amounts of melanin at an irregular pace [4]. For instance, melanin is produced when powerful UV radiation from sunlight is exposed for a prolonged period [5].

Melanoma, a fatal form of skin cancer, is caused by the abnormal growth of melanocytes [6]. Early melanoma detection is crucial for adequate therapy [7]. The five-year survival rate for melanoma is around 92% if it is discovered sooner. The primary challenge in melanoma identification is the visual

comparison of benign and malignant skin lesions [8]. Due to this, even an experienced specialist finds the melanoma detection procedure difficult [9, 10]. Dermoscopy is one of the imaging techniques used in modern times, among others [11, 12].

CAD technology is essential to help the experts in the diagnosis procedure in detecting melanoma [13]. Because skin lesion images have such a wide range in position, color, size, and texture, segmenting them is a challenging process [14, 15]. Additionally, the poor contrast of the images makes it impossible for us to detect differences between surrounding tissues [16, 17]. Extra features such as air bubbles, ebony frames, color lighting, ruler markings, and blood vessels complicate lesion segmentation [18].

Different imaging modalities and procedures segment skin lesions [19]. In deep learning (DL), skin lesion identification using convolutional neural networks (CNN) techniques has been successful in

recent years. In the network, the number of variables and estimations are reduced by accepting the lower-resolution images in the CNN model [20]. CNN models have demonstrated exceptional accuracy in classifying skin lesions. They often outperform dermatologists accurately, especially when trained on large and diverse datasets. This research proposes an integrated deep-learning network model for skin cancer classification. The improved CapsNet model for extracting significant features of the image. EOPNN classifier is employed for skin lesion classification. The classifier's parameters are updated using the IAJO algorithm to improve the classification performance. Using a well-known dataset of skin color images like ISIC2017, the suggested approach was tested and evaluated.

Following is the format for the remaining sections of the paper; section 2 summarizes earlier work on dermoscopy image-based skin lesion classification. The methods used to create the DL predictive model are described in section 3. Section 4 provides instances illustrating the experimental findings for each stage. The research's significant findings are effectively summarized in section 5.

### 1.1 Major contribution

- For the detection and classification of skin lesions, this research proposes a novel integrated deep learning network model-based CAD technique known as EOPNN-IAJO.
- The two phases of image pre-processing used by the EOPNN-IAJO model are hair removal using the dull razor technique and noise reduction using average median filtering.
- The Otsu thresholding approach is combined with a mathematical morphology-based segmentation methodology to identify the areas of infected lesions in dermoscopic images.
- The efficient features of the dermoscopy images are extracted using improved CapsNet, which has convolution blocks and multi-stage structures at each level.
- For multi-class skin cancer classification, the deep learning-based EOPNN model is used. It classifies the dermoscopy images into melanoma (MV), seborrheic keratosis (SV), and nevus (NV), respectively. IAJO method was used to select the smoothing parameter of ANN in the best possible manner.
- A comprehensive simulation analysis was conducted using the benchmark ISIC dataset to examine the EOPNN-IAJO model's effectiveness in classifying skin lesions. The experiments are performed on the Python platform. Experimental

results show that the proposed approach outperforms the state efficiency of all previous approaches.

## 2. Related works

For dermoscopy image segmentation, a hyper-parameter optimized fully convolution encoder-decoder network (FCEDN) was developed by Mohakud et al. [21]. A unique approach called exponential neighborhood grey wolf optimization (EN-GWO) optimizes the network's hyper-parameters.

For skin melanoma segmentation, faster RCNN and fuzzy k-means clustering (FKM) are employed by Nawaz et al. [22]. For attaining a fixed-length feature vector, the illumination and noise problems are removed. The melanoma-affected skin area has been separated into segments using FKM, which has variable boundaries and sizes.

For skin cancer classification, a deep learning model is presented by Hosny et al. [23]. There are three primary phases in the described technique. In the pre-processing stage, the affected region is segmented. Rotation and Translation modifications are used in the data augmentation step in the segmented ROI images. Then, several DCNN designs are used for classification.

A DSCC\_Net, which is based on a CNN, was proposed by Tahir et al. [24]. Dermoscopy images may extract dominating characteristics that the suggested model can use to help accurately identify the condition. Using the Grad-CAM heat map technique, the visual characteristics of techniques for skin cancer classifications are illustrated.

For the early identification of skin cancer, a novel approach was published by Tabrizchi et al. [25] based on the analysis of dermoscopic images. The VGG-16 network, based on the well-known CNN architecture, serves as the model's foundation. A modified VGG network model is used for skin cancer detection.

For precise skin cancer identification, Femil et al. [26] use a successful image-processing strategy. The affected region segmentation is done using the cascaded FCM approach. The PNN classifier helps substantially categorize the characteristics to categorize skin lesions' phases accurately.

The challenges of existing related works are given in Table 1. The major difficulties of the existing related works on skin cancer classification are (1) data domain inconsistency leads to slow convergence and (2) limited resistance to unclear skin lesions. For effective skin cancer classification, we propose an efficient, integrated, optimized deep-learning network model to solve these problems.

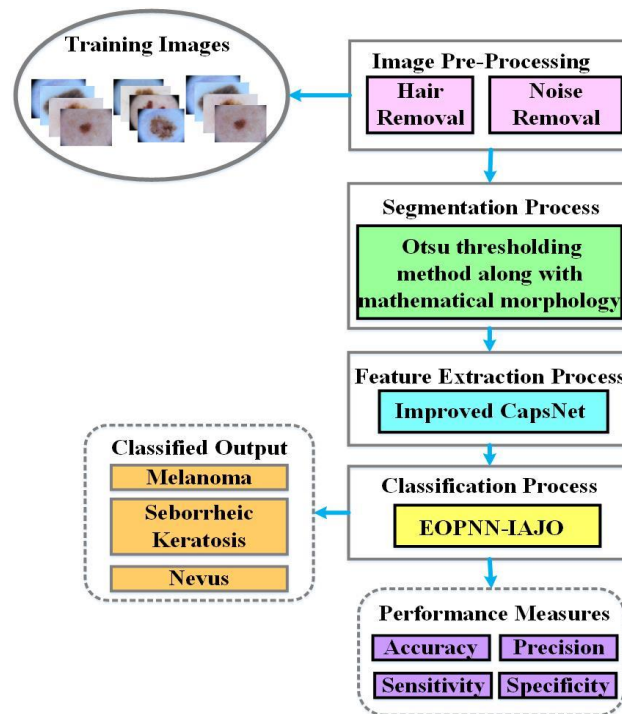


Figure. 1 Schematic diagram of the proposed methodology

Table 1. Literature Survey

Reference	Year	Model	Difficulties
Mohakud et al. [21]	2022	FCEDN	This model will decrease its classification accuracy in cases where the number of classes is very high
Nawaz et al. [22]	2022	Faster RCNN	It lowers the rate of classification recognition
Hosny et al. [23]	2020	DCNN	High computer resources are needed for training with high-resolution data.
Tahir et al. [24]	2023	DSCC-Net	It produces final results with poor-quality images
Tabrizchi et al. [25]	2022	VGG-16	It Requires additional time for training and a highly complex process
Femil et al. [26]	2023	PNN	It lowers the classifier quality in real-time applications.

### 3. Proposed methodology

The operational phase of the proposed EOPNN-IAJO model is shown in Fig. 1. Pre-processing, segmentation, feature extraction, and classification are the four processes that comprise our method's

overall framework. Processes such as removing hair with a dull razor and removing noise with an average median filter are used during image pre-processing. In the dermoscopic images, the affected lesion regions are segmented using the Otsu thresholding approach in conjunction with a mathematical morphology-based segmentation strategy. The improved CapsNet model takes the segment images of skin lesions to extract the image's significant features. The EOPNN classifier is employed for classifying the skin images into melanoma (MV), seborrheic keratosis (SV), and nevus (NV), respectively. IAJO is used for updating the parameters of the EOPNN classifier, which improves the classification performance.

#### 3.1 ISIC 2017 dataset

To determine our method of estimation, we utilize the ISIC 2017 dataset. Nevus, seborrheic keratosis, and melanoma are three groups of dermatological images included in the ISIC 2017 dataset, as indicated in Table 2. In the dataset, a total of 2750 images are present. The dataset images are divided into three sections for experimental analysis. Two thousand images are used for the training set, 150 images are used for the validation set, and 600 images are used for the test set. The efficiency of the proposed approach is demonstrated by performing more ablation experiments using the ISIC 2017 dataset in this research. Additionally, we compared our proposed approach to various baseline

Table 2. Dataset distribution of the ISIC 2017 dataset

	Melanoma	Keratosis	Nevus	Total
Training	374	254	1372	2000
Validation	30	42	78	150
Testing	117	90	303	600

approaches.

### 3.2 Image pre-processing

Pre-processing: The procedure for image capture must not be uniform in several respects. The image's undesired portions are reduced or removed using efficient pre-processing steps to enhance the image parameters like clarity and quality. The primary pre-processing procedures include hair removal and noise removal. The average median filters are used for image enhancement and noise removal. The Dull Razor Method is performed with filters to remove unwanted hair from the skin lesion.

Image enhancement seeks to improve the quality of the image by making it more visible. Typically, body hair is present in most skin lesions, which might make it difficult to classify them with high precision. Therefore, the dull razor approach eliminates the undesirable hair from the photos. The dull razor technique mostly does these operations: a) on the skin lesion, the exact position of the hair can be determined utilizing the grayscale morphological operation. b) It first determines if the form is a long or thin structure, then locates the hair pixel's position and replaces it using bilinear interpolation. c) Finally, it uses an adaptive median filter to smooth the replacement hair pixel.

### 3.3 Image segmentation

The area of interest (ROI) is determined using the Otsu thresholding approach and mathematical morphology. To provide segmentation results with less complexity, low-cost segmentation is offered by our Otsu segmentation approach. The Otsu approach automates the segmentation of the input pictures by reducing intragroup variation and optimizing intergroup variance. When the background resolution of a picture is inadequate, global thresholding might have some issues (heterogeneity impact). Local thresholding is employed to enhance this impact. The class-in-between variance is reduced using the threshold value, which is analyzed according to the Otsu thresholding approach. This is accomplished using the below equation:

$$\sigma_w^2(t) = \omega_1(t)\sigma_1^2(t) + \omega_2(t)\sigma_2^2(t) \quad (1)$$

Where the variation within the groups is represented by the value  $\sigma_i^2$ . In two separate groups, the probability with magnitude  $t$  is represented by  $W$ . The class variance reduction is equivalent to class-within-class variance maximization according to the Otsu technique.

$$\sigma_b^2(t) = \sigma^2 - \sigma_w^2(t) = \omega_1(t)\omega_2(t)[\mu_1(t) - \mu_2(t)]^2, \quad (2)$$

Where  $\mu_i$  represents the mean value.

Based on mathematical morphology, the accuracy of the segmentation is then increased using three post-processing methods. Mathematical filling, closing, and opening are used in the three processes. The constructing element is depicted as  $B$ , and the processed area is denoted as  $A$ . Without affecting the remaining image elements, the following step involves using a mathematical opening to eliminate unnecessary, inexpensive information. The following is a model for the mathematical opening:

$$A \circ B = (A \ominus B) \oplus B \quad (3)$$

The following equation connects the narrow portions by using mathematical closure:

$$A \cdot B = (A \oplus B) \ominus B \quad (4)$$

### 3.4 Feature extraction using improved CapsNet model

From the segmented image, a feature extraction method is used to extract several beneficial feature vectors after completing image segmentation. As a feature extractor, the improved CapsNet model is employed for improving the classification performance. When manually processed via an attribute or variable selection method, the fused vector (FV) outputs could include redundant or unneeded features. A selection from the deeply significant parameters is the entire feature selection process. The uncertain data is assessed using the concept of entropy in the proposed work, and the system disorder is presented by showing the unpredictability of the signal.

For preserving feature information and object position in an image and modeling relationships between objects, the CapsNet model is created. Utilizable information from the information enters before the pooling layer in the CNN approach. The neural result of the CNN technique also produces a scalar value. Many neurons are used for forming capsules. Vector output of comparable size but with different routing is provided by using CapsNets. The

variable of images is shown by vector routing [20]. The CNN uses sigmoid scalar, ReLU, and tangent input activation functions. A function for vector activation is used by the CapsNet feature extraction network called squashing, as defined in Eq. (1).

$$v_j = \frac{\|S_j\|^2 S_j}{1 + \|S_j\|^2 \|S_j\|} \quad (5)$$

Where overall capsule input is represented as  $j$ , and  $S_j$  the capsule output is represented as  $v_j$ . Whenever an object appears in the picture, the lengthy vector  $v_j$  shrinks to one. The choke shorter vector becomes 0 without an object in the image. In addition to CapsNet's first layer, the predicted vector ( $U_{j|i}$ ) in the capsule's average weight, which is positioned in the bottom layer, estimates the total input values of the capsule  $S_j$ . A weight matrix ( $W_{ij}$ ) and lower layer capsule's output ( $O_i$ ) are used to determine the predictive vector ( $U_{j|i}$ ).

$$S_j = \sum_i b_{ij} u_{j|i} \quad (6)$$

$$u_{j|i} = W_{ij} O_i \quad (7)$$

Where the dynamic routing procedure's coefficient is indicated by the  $b_{ij}$ , and it is given by,

$$b_{ij} = \frac{\exp(a_{ij})}{\sum_k \exp(a_{ik})} \quad (8)$$

Where log-likelihood is indicated by  $a_{ij}$  Softmax's definition of the log prior probability, and the capsules  $i$  and those in the top layer have a one correlation coefficient. CapsNet offers a margin loss for identifying the objects of a specific class that are present and is estimated as follows,

$$L_k = T_k \max(O, m^+ - \|v_k\|)^2 + \lambda(1 - T_k \max(O, \|v_k\| - m^-)^2) \quad (9)$$

When class  $k$  is present,  $T_k$  it has a value of 1. The weight of the loss is represented by,  $m^- = 0.1$  and hypervariable is represented by  $m^+ = 0.9$ . The probability in the section of the image is denoted by the vector length, which is calculated using CapsNet. The image's texture, color, location, size, and other information are included in the vector direction.

### 3.5 Image classification

When completing the classification process in its final step, the EOPNN-IJOA approach is employed

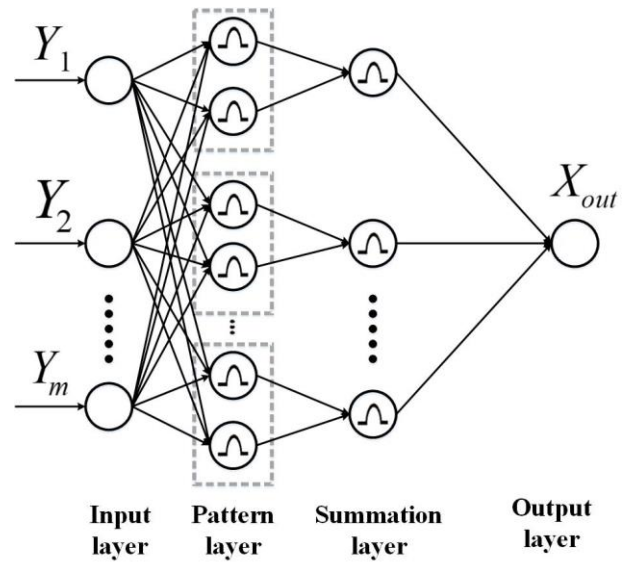


Figure. 2 Structure of EOPNN

to assign class labels efficiently.

#### 3.5.1. Network structure of EOPNN classifier

The classification network model. In the possibility category, dermoscopy pictures' retrieved features are used as input in the categorization procedure. To distinguish between the standard and unusual types of dermoscopy images, an EOPNN classifier is utilized. It has a perplexing structure and resembles a feed-forward neural network. The bayes request rule and parzen nonparametric probability density function (PDF) assessment are used directly in the neural organization of the EOPNN structure. In particular, the input, design, summation, and output layers are present in the enhanced version of the radial basis transfer function serves as the input of the vector class of the EOPNN with maximum accuracy. The EOPNN classifier's weight evaluations are certainly selected using IAJO to update the EOPNN classifier. Fig. 2 shows the EOPNN classifier's organizational structure.

**Step 1:** The input layer is initially provided with the inputs. In the input layer, the input vector size and number of neurons are equal. The input neurons receive the training sample  $Y = (y_1, y_2, \dots, y_m)^T$ , which is then sent to the pattern layer.

**Step 2:**  $S$  groups are used to classify the neurons in the pattern layer, one for each class, after the information layer's sample transmission. After the radial basis nonlinear planning, the distance between the weight vector  $W$  and preparing tests  $Y$  is computed using the pattern layer and obtains the yield vector  $N$ . The spiral premise work is often chosen using the Gaussian capacity. The equation following

describes the Gaussian kernel shape that the  $j^{th}$  pattern neuron in the  $i^{th}$  group uses to register its yield.

$$N_{ji}(Y) = \frac{1}{(2\pi\sigma^2)^{m/2}} \exp\left[-\frac{\|Y-W_{ji}\|^2}{2\sigma^2}\right] \quad (10)$$

Where  $\sigma$  represented as a smoothening parameter.

**Step 3:** Combining the newly discovered densities, the EOPNN classifier's summation layer estimates the contingent class probability capacity.

$$R_j(Y) = \sum_{j=1}^M w_{ji} N_{ji}(Y), j \in \{1,2,\dots,m\} \quad (11)$$

Where the mixed weights are represented as  $w_{ji}$  and subject to

$$\sum_{j=1}^M w_{ji} = 1, j \in \{1,2,\dots,m\} \quad (12)$$

Where;

$m \rightarrow$  Overall number of patterns

$M_j \rightarrow$  Neurons in the  $j^{th}$  pattern layer in terms of the number

**Step 4:** The output is produced by the last layer of the EOPNN output layer.

$$O(Y) = \arg \max_{1 \leq j \leq m} (R_j) \quad (13)$$

IAJO algorithm is used for optimally selecting the smoothing parameter  $\sigma$  for improving the classification performance.

### 3.5.2. EOPNN parameter optimization using IAJO algorithm

The smoothing parameter's optimal value is defined by using one of the powerful optimization algorithms like the IAJO algorithm. Around the world, jellyfish are found in seas with varying temperatures and pressures. The three criteria listed below serve as a basis for the IAJO algorithm's operation;

- The "time control mechanism" allows jellyfish to alternate between following ocean currents and moving inward.
- In pursuit of food, jellyfish wander the water. Where there is more food available, they are more attracted.
- The related objective activities and location determine the amount of food identified.

Below is a detailed description of the parameter

optimization method;

**Step 1:** Solution encoding: When using EOPNN, the smoothing parameter  $\sigma$  is first randomly assigned. All optimization techniques need solution encoding. A jellyfish analogy is used for each parameter. The  $Y$  is used to represent this solution.

**Step 2:** Objective function evaluation: Each solution's objective function is assessed following the solution encoding procedure. The fitness function (FF) is commonly thought of as classification accuracy.

$$FF = \text{Maximum}(\text{Accuracy}) \quad (14)$$

**Step 3:** Utilizing an improved jellyfish algorithm for network improvement: The ocean current direction is computed after the fitness computation. A significant number of nutrients are present in the ocean current. Jellyfish are attracted to areas with high nutrition levels.

$$\vec{D} = \frac{1}{N_{Pop}} \sum \vec{D}_i = \frac{1}{N_{Pop}} \sum (Y^* - E_c Y_i) = Y^* - E_c \frac{\sum Y_i}{N_{Pop}} \quad (15)$$

$$= Y^* - E_c \mu$$

$$\text{Set } df = E_c \mu$$

The below equation is used for the calculation of  $\vec{D}$  finally,

$$\vec{D} = Y^* - df \quad (16)$$

Where,

$df \rightarrow$  Differentiate between the jellyfish's present optimal position and their average location.

$\mu \rightarrow$  The mean value of jellyfish

$E_c \rightarrow$  The factor of attraction

$Y^* \rightarrow$  The best position for jellyfish

$N_{Pop} \rightarrow$  Number of jellyfish

The following equation indicates the jellyfish's new location.

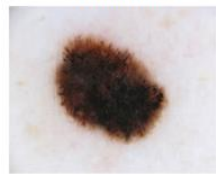



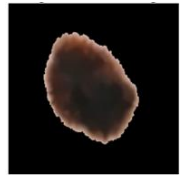





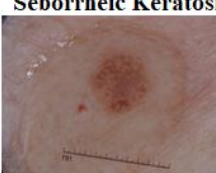




$$Y_i(k+1) = Y_i(k) + \text{rand}(0,1) \times \vec{D} \quad (17)$$

The improved solutions are based on the equations above.

**Step 4:** Termination criteria: Once the best wellness esteem has been selected, the algorithm stops presenting. When IAJO techniques result in the most significant level of well-being, special consideration is given to the EOPNN classifier.



Figure. 3 Experimental results of the proposed approach to skin lesion detection

Input Image	Hair removal Image	Noise Removal Image	Ground Truth	Segmented Image
<b>Melanoma</b> 				
<b>Nevus</b> 				
<b>Seborrheic Keratosis</b> 				

#### 4. Result and discussion

On the skin lesion ISIC 2017 dataset, the proposed approach's efficiency is performed by ablation experiments. We also contrasted our technique with various existing approaches on the ISIC 2017 dataset. The datasets were split into three sections for experiment analysis: 72% for training, 8% for validation, and 20 % for testing.

##### Performance validation

The benchmark skin lesion ISIC 2017 dataset is used to validate the effectiveness of the provided technique's skin lesion classification. The presented approaches' parameter settings are kernel size: 3, filter size: 32, learning rate: 0.001, number of epochs: 50, batch size: 148, L2 normalization term: 0.001, and number of hidden feature layers: 128. F1-Measure, precision, accuracy, specificity, and sensitivity are a group of metrics used to assess performance.

$$Sensitivity = \frac{TP}{FN+TP} \tag{19}$$

$$Specificity = \frac{TN}{FP+TN} \tag{20}$$

$$Accuracy = \frac{TN+TP}{FN+FP+TN+TP} \tag{18}$$

$$Precision = \frac{TP}{FP+TP} \tag{19}$$

Where false negative, false positive, true negative,

and true positive are denoted as FN, FP, TN, and TP

#### 4.1 Experimental results

The suggested deep learning model, the Net model, was implemented using Keras. Additionally, Python was used to program the methods that were not immediately related to convolutional networks. Using a PC with 32 GB RAM, 11 GB NVIDIA GPU, and an operating system of Windows 10, the experiment was carried out.

The assessment criteria for the experimental findings are mostly taken from the confusion matrix as we evaluate our approach using the test dataset. Specificity, sensitivity, accuracy, and area under the curve (AUC) are used for evaluating our proposed approach for skin cancer classification on the ISIC 2017 dataset. The initial 200 cases (EOPNN-IAJO) with the most significant loss are chosen as the perplexing examples in our suggested deep learning technique. The original examples are divided by the confusing examples at a ratio of 2:1. Up to 50 epochs of training with the EOPNN-IAJO were conducted. The experimental results of the proposed approach to skin cancer classification are given in Fig. 3.

Seborrheic keratosis and melanoma are the two primary undefinable classes in ISIC 2017, with melanoma being a skin condition that threatens human health and life. Table 3 displays the average findings and the categorization results for melanoma, nevus, and seborrheic keratosis. The proposed approach produces higher results in performance

Table 3. Results of classifying the ISIC 2017 test set

Classes	Accuracy (%)	Sensitivity (%)	Specificity (%)	Precision (%)
Melanoma	99.62	99.05	98.85	98.89
Nevus	99.23	99.03	99.43	99.23
Seborrheic Keratosis	99.67	99.00	99.57	99.67
Average	99.53	99.02	99.23	99.26

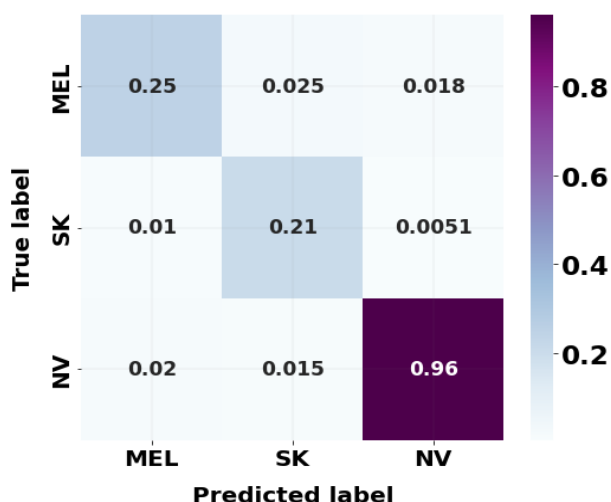


Figure. 4 Confusion matrix on ISIC 2017 dataset

measures. High-performance classification results make more accurate and reliable decisions, reducing the probability of incorrect predictions. In skin cancer diagnosis, high-performance classification results can assist healthcare professionals in detecting diseases and conditions more accurately and at earlier stages, potentially leading to better patient outcomes.

The normalized confusion matrices for the suggested technique on the ISIC 2017 testing set are shown in Fig. 4. Melanoma, seborrheic keratosis, and nevus are called MEL, SK, and NV, respectively. Without utilizing external training data, the findings demonstrate that the proposed approach may provide a superior classification outcome for the classification of skin cancer. Compared to previous approaches, our method outperforms them in AUC and ACC while balancing the performance of SE and SP.

The training and validation accuracy graph of EOPNN-IAJO on the ISIC 2017 dataset is represented in Fig. 5. On our private dataset, our suggested model had an accuracy of 99.53%. 99.53% accuracy is achieved for training and 99.50% for validation on our dataset after 50 epochs. On the ISIC 2017 dataset, outstanding performance is achieved by

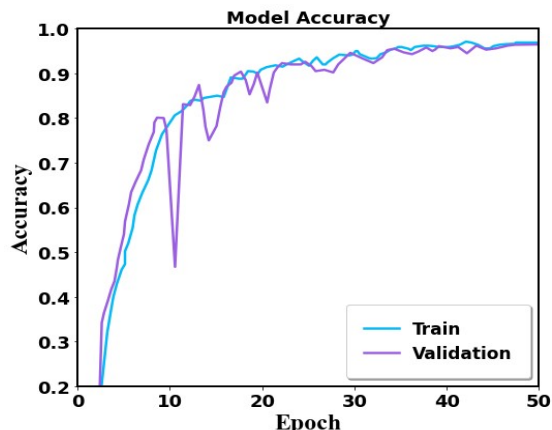


Figure. 5 The ISIC 2017 dataset's EOPNN-IAJO training accuracy versus validation accuracy graph

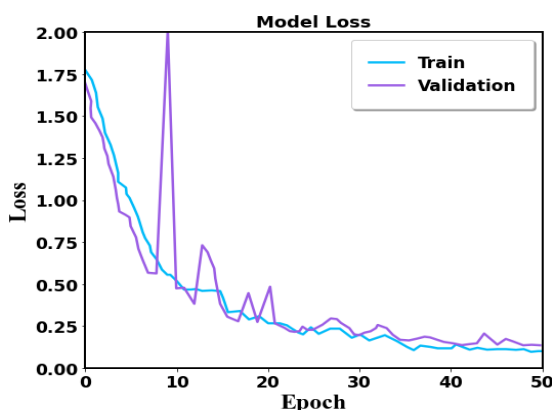


Figure. 6 The ISIC 2017 dataset's EOPNN-IAJO training loss versus validation loss graph

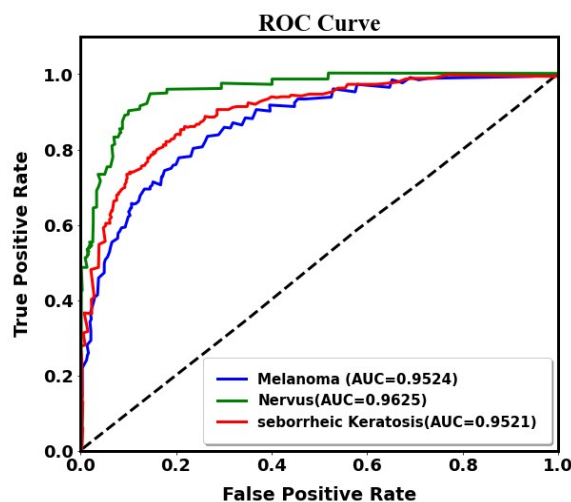


Figure. 7 ROC Curve on ISIC 2017 dataset

our proposed approach in both the training set and the testing set after analyzing the various epoch settings. For using the proposed EOPNN-IAJO approach, the training and validation loss graph is shown in Fig. 6. The final validation loss of 0.23 and training loss of 0.23 are achieved by the proposed EOPNN-IAJO approach, with the loss rising with each succeeding epoch. With the aid of the 50 epochs of the example,



Table 4. Performance evaluation using ISIC 2017 dataset

Reference	Year	Method	Sensitivity (%)	Specificity (%)	Accuracy (%)
Mohakud et al. [21]	2022	FCEDN	-	-	95.25
Hosny et al. [23]	2020	Modified GoogleNet	97.27	98.60	98.14
Deng et al. [27]	2022	Resnet152-HRL	74	96.1	85.8
Kaur et al. [28]	2022	DCNN	89.25	88.86	88.23
Bibi et al. [29]	2022	C-SVM	-	-	96.70
Cirrincone et al. [30]	2023	ViT-based model	92.80	96.70	94.08
<b>Proposed Approach</b>		EOPNN-IAJO	99.02	99.23	99.53

our algorithm has worked remarkably well on our dataset, with reasonable accuracy and minimum loss. Fig. 7 shows the AUC-ROC graph for the suggested method of classifying skin lesions.

#### 4.2 Performance evaluation

The existing models require large amounts of high-quality labeled data to perform effectively. Gathering such data can be challenging, especially for less common types of skin cancer. In some cases, the data may be imbalanced, with more examples of one type of skin lesion than others. The existing models produce more false positives and negatives, affecting the classification performance. The existing models produce higher results for binary classification, but multi-classification introduces additional complexity. However, our proposed approach produces less number of false positives and false negatives, which can increase the overall classification performance. The suggested method accelerates the training of confusing samples and prevents slow convergence caused by the inconsistent data domain. The proposed approach performs better than other approaches in the ISIC 2017 dataset without the need for additional data.

Table 4 compares the performance of our deep learning-based EOPNN-IAJO technique with other cutting-edge approaches that also employ the ISIC 2017 dataset. For dermoscopy image segmentation, Mohakud et al. [21] explored a hyper-parameter-optimized FCEDN; a unique approach called exponential neighborhood grey wolf optimisation (EN-GWO) optimizes the network's hyper-parameters; it has an overall accuracy of 95.25%. To classify skin diseases, Hosny et al. [23] examined a modified GoogleNet model, which produces an

accuracy of 98.14%. A hierarchical representation learning approach based on an efficient structural pseudo inverse learning is developed by Deng et al. [27]; it produces a maximum accuracy of 85.8%. An automated melanoma classifier based on a DCNN was developed by Kaur et al. [28]; it achieves an overall accuracy of 88.23%. Bibi et al. [29] developed an effective deep-learning framework for skin cancer classification; the classification uses a cubic SVM, achieving an overall accuracy of 96.70%. To distinguish between melanoma and non-cancerous lesions, a ViT-based design was described by Cirrincone et al. [30]; it attains a maximum accuracy of 94.80%.

The proposed deep learning-based model (EOPNN-IAJO) produces better results in classifying skin lesion images than the existing models. This increase is explained by the model's capability to efficiently acquire and represent the image's spatial relationships with long-range. The proposed experiments demonstrate excellent classification results on the given dataset by correctly classifying images from all three categories. Compared to other models, the specificity of 99.23%, the sensitivity of 99.02%, and the accuracy of 99.53% were much higher. This is because EOPNN's parameters were optimized. The EOPNN classifier's classification accuracy is improved using the IAJO algorithm.

The suggested architectural approach compromises classification performance and computational cost. The research done during the hyper-parameter tuning phase led to a prediction model with extremely high specificity and sensitivity, resulting in very little false positive data (positive and negative). The data over-fitting problem is also solved by the proposed deep learning approach. This was supported by our ablation analysis as well,

demonstrating that not all layers are necessary. The image's most abstract relationships are represented by the last layer of the classification network on the model; it may be inferred that the low-level properties of the image are all that is needed for the superior classification keys.

Though the suggested method produces superior outcomes at convergence, the training's dynamics (see Fig. 6) must be revised since there are significant peaks. The internal covariate and small size of the mini-batches change were likely to blame for this phenomenon. To address this issue, future research will focus on regularization strategies, including generative networks (e.g., GANs and diffusers) used for data augmentation.

## 5. Conclusion

This research develops an innovative EOPNN-IAJO model to identify and classify skin lesions from dermoscopic images. The EOPNN-IAJO model encompasses image pre-processing, image segmentation using the Otsu thresholding method and mathematical morphology, feature extraction using improved CapsNet-based, and classification using EOPNN-IAJO. Following pre-processing of the raw dermoscopic images, the segmentation of lesion regions is performed utilizing the Otsu thresholding approach and mathematical morphology. A feature extractor is then used with the improved CapsNet model. However, the improved CapsNet features were retrieved at a higher level, and multi-labeled predictions were provided by sending these features immediately to the EOPNN classifier. By recurrent feeding with comparable characteristics, the higher-order probabilistic dependency cannot be learned by this. The classification procedure is completed using the EOPNN-IAJO model, and effective class labels are assigned. IAJO is used for selecting smoothing parameters optimally to improve the performance of the EOPNN classifier. The suggested framework outperformed existing models in accuracy, sensitivity, and specificity, achieving 99.53%, 99.02%, and 99.23% %, respectively. In the future, machine learning algorithms with optimization models can be used to build early-stage skin cancer detection approaches, and the effectiveness of the suggested approach may be evaluated using a sizable dataset and IoT-enabled environment.

## Conflicts of interest

The authors declare that they have no known competing financial interests or personal relationships that could have appeared to influence

the work reported in this paper.

## Author contributions

Conceptualization, Vankayalapati Radhika and Sai Chandana; methodology, Vankayalapati Radhika; software, Sai Chandana; validation, Vankayalapati Radhika and Sai Chandana; formal analysis, Sai Chandana; investigation, Vankayalapati Radhika; resources, Sai Chandana; writing—original draft preparation, Vankayalapati Radhika; writing—review and editing, Sai Chandana.

## Acknowledgment

We declare that this manuscript is original, has not been published before, and is not currently being considered for publication elsewhere.

## Reference

- [1] A. Mahbod, G. Schaefer, C. Wang, G. Dorffner, R. Ecker, and I. Ellinger, "Transfer learning using a multi-scale and multi-network ensemble for skin lesion classification", *Computer Methods and Programs in Biomedicine*, Vol. 193, p. 105475, 2020.
- [2] M. A. Kassem, K. M. Hosny, and M. M. Fouad, "Skin lesions classification into eight classes for ISIC 2019 using deep convolutional neural network and transfer learning", *IEEE Access*, Vol. 8, pp. 114822-114832, 2020.
- [3] Z. Rahman, M. S. Hossain, M. R. Islam, M. M. Hasan, and R. A. Hridhee, "An approach for multi-class skin lesion classification based on ensemble learning", *Informatics in Medicine Unlocked*, Vol.25, p. 100659, 2021.
- [4] J. Saeed and S. Zeebaree, "Skin lesion classification based on deep convolutional neural network architectures", *Journal of Applied Science and Technology Trends*, Vol. 2, No. 01, pp. 41-51, 2021.
- [5] S. Ayas, "Multi-class skin lesion classification in dermoscopic images using swin transformer model", *Neural Computing and Applications*, Vol. 35, No. 9, pp. 6713-6722, 2023.
- [6] J. A. A. Damian, V. Ponomaryov, S. Sadovnychiy, and H. C. Fernandez, "Melanoma and nevus skin lesion classification using handcraft and deep learning feature fusion via mutual information measures", *Entropy*, Vol. 22, No. 4, p. 484, 2020.
- [7] S. R. Salian and S. D. Sawarkar, "Melanoma skin lesion classification using improved efficientnetb3", *Jordanian Journal of Computers and Information Technology*, Vol. 8,

- No. 1, 2022.
- [8] R. Rout, P. Parida, and S. Dash, "Automatic Skin Lesion Segmentation using a Hybrid Deep Learning Network", *International Journal of Computer Information Systems and Industrial Management Applications*, Vol. 15, pp. 238-249, 2023.
- [9] P. Tang, Q. Liang, X. Yan, S. Xiang, and D. Zhang, "GP-CNN-DTEL: Global-part CNN model with data-transformed ensemble learning for skin lesion classification", *IEEE Journal of Biomedical and Health Informatics*, Vol. 24, No. 10, pp. 2870-2882, 2020.
- [10] S. Khoulood, M. Ahlem, T. Fadel, and S. Amel, "W-net and inception residual network for skin lesion segmentation and classification", *Applied Intelligence*, pp. 1-19, 2022.
- [11] M. K. Hasan, L. Dahal, P. N. Samarakoon, F. I. Tushar, and R. Martí, "DSNet: Automatic dermoscopic skin lesion segmentation", *Computers in Biology and Medicine*, Vol. 120, p. 103738, 2020.
- [12] M. A. Anjum, J. Amin, M. Sharif, H. U. Khan, M. S. A. Malik, and S. Kadry, "Deep semantic segmentation and multi-class skin lesion classification based on convolutional neural network", *IEEE Access*, Vol. 8, pp. 129668-129678, 2020.
- [13] S. Ding, Z. Wu, Y. Zheng, Z. Liu, X. Yang, X. Yang, G. Yuan, and J. Xie, "Deep attention branch networks for skin lesion classification", *Computer Methods and Programs in Biomedicine*, Vol. 212, p. 106447, 2021.
- [14] T. Akram, H. M. J. Lodhi, S. R. Naqvi, S. Naeem, M. Alhaisoni, M. Ali, S. A. Haider, and N. N. Qadri, "A multilevel features selection framework for skin lesion classification", *Human-Centric Computing and Information Sciences*, Vol. 10, pp. 1-26, 2020.
- [15] S. Benyahia, B. Meftah, and O. Lézoray, "Multi-features extraction based on deep learning for skin lesion classification", *Tissue and Cell*, Vol. 74, p. 101701, 2022.
- [16] H. Wu, S. Chen, G. Chen, W. Wang, B. Lei, and Z. Wen, "FAT-Net: Feature adaptive transformers for automated skin lesion segmentation", *Medical Image Analysis*, Vol. 76, p. 102327, 2022.
- [17] P. Chen, S. Huang, and Q. Yue, "Skin lesion segmentation using recurrent attentional convolutional networks", *IEEE Access*, Vol. 10, pp. 94007-94018, 2022.
- [18] L. Yang, C. Fan, H. Lin, and Y. Qiu, "Rema-Net: An efficient multi-attention convolutional neural network for rapid skin lesion segmentation", *Computers in Biology and Medicine*, Vol. 159, p. 106952, 2023.
- [19] Z. Yu, L. Yu, W. Zheng, and S. Wang, "EIU-Net: Enhanced feature extraction and improved skip connections in U-Net for skin lesion segmentation", *Computers in Biology and Medicine*, p. 107081, 2023.
- [20] R. Kaur and S. K. Ranade, "Improving accuracy of convolutional neural network-based skin lesion segmentation using group normalization and combined loss function", *International Journal of Information Technology*, pp. 1-9, 2023.
- [21] R. Mohakud and R. Dash, "Skin cancer image segmentation utilizing a novel EN-GWO based hyper-parameter optimized FCEDN", *Journal of King Saud University-Computer and Information Sciences*, Vol. 34, No. 10, pp. 9889-9904, 2022.
- [22] M. Nawaz, Z. Mehmood, T. Nazir, R. A. Naqvi, A. Rehman, M. Iqbal, and T. Saba, "Skin cancer detection from dermoscopic images using deep learning and fuzzy k-means clustering", *Microscopy Research and Technique*, Vol. 85, No. 1, pp. 339-351, 2022.
- [23] K. M. Hosny, M. A. Kassem, and M. M. Foad, "Skin melanoma classification using ROI and data augmentation with deep convolutional neural networks", *Multimedia Tools and Applications*, Vol. 79, pp. 24029-24055, 2020.
- [24] M. Tahir, A. Naeem, H. Malik, J. Tanveer, R. A. Naqvi, and S. W. Lee, "DSCC\_Net: Multi-Classification Deep Learning Models for Diagnosing of Skin Cancer Using Dermoscopic Images", *Cancers*, Vol. 15, No.7, p. 2179, 2023.
- [25] H. Tabrizchi, S. Parvizpour, and J. Razmara, "An improved VGG model for skin cancer detection", *Neural Processing Letters*, pp. 1-18, 2022.
- [26] J. J. Femil and T. Jaya, "An Efficient Hybrid Optimization for Skin Cancer Detection Using PNN Classifier", *Computer Systems Science & Engineering*, Vol. 45, No. 3, 2023.
- [27] X. Deng, Q. Yin, and P. Guo, "Efficient structural pseudoinverse learning-based hierarchical representation learning for skin lesion classification", *Complex & Intelligent Systems*, Vol. 8, No. 2, pp. 1445-1457, 2022.
- [28] R. Kaur, H. G. Hosseini, R. Sinha, and M. Lindén, "Melanoma classification using a novel deep convolutional neural network with dermoscopic images", *Sensors*, Vol. 22, No. 3, p. 1134, 2022.
- [29] A. Bibi, M. A. Khan, M. Y. Javed, U. Tariq, B. G. Kang, Y. Nam, R. R. Mostafa, and R. H. Sakr,

“Skin lesion segmentation and classification using conventional and deep learning-based framework”, *Comput. Mater. Contin*, Vol. 71, pp. 2477-2495, 2022.

- [30] G. Cirrincione, S. Cannata, G. Cicceri, F. Prinzi, T. Currieri, M. Lovino, C. Militello, E. Pasero, and S. Vitabile, “Transformer-Based Approach to Melanoma Detection”, *Sensors*, Vol. 23, No. 12, p. 5677, 2023.